



CO₂ absorption in aqueous NH₃ solutions: Novel dynamic modeling of experimental outcomes

Federico Atzori^{a,*}, Francesco Barzagli^b, Alberto Varone^a, Giacomo Cao^{a,c,d},
Alessandro Concas^{c,d,*}

^a Center for Advanced Studies, Research and Development in Sardinia (CRS4), Loc. Piscina Manna, Building 1, 09050 Pula (CA), Italy

^b National Research Council (CNR), ICCOM Institute, via Madonna del Piano 10, 50019 Sesto F.no, Florence, Italy

^c Department of Mechanical, Chemical and Materials Engineering, University of Cagliari, Piazza d'Armi, 09123 Cagliari, Italy

^d Interdepartmental Center of Environmental Science and Engineering (CINSA), University of Cagliari, Via San Giorgio 12, 09124 Cagliari, Italy

ARTICLE INFO

Keywords:

Capture
Dynamic modeling
Chemical absorption
Aqueous ammonia process
Gas/liquid mass transfer

ABSTRACT

It is well known that CO₂ capture and re-use is one of the main challenges to be pursued in order to tackle global warming issues. Aqueous ammonia solutions are among the most promising sorbents for post-combustion CO₂ capture and could represent a valid and potentially economical alternative to the use of conventional alkanolamines, due to their higher absorption capacity, lower energy requirements for sorbent regeneration and greater resistance to oxidative and thermal degradation. Despite its apparent simplicity and convenience, the dynamic evolution of CO₂ – NH₃ system needs to be further investigated through proper mathematical models that permit to design, optimize, and control the capture process.

In this work, the chemical absorption of carbon dioxide contained in a simulated flue gas (N₂ + CO₂; CO₂ 15%_{v/v}) by means of aqueous NH₃ solutions was investigated both experimentally and theoretically. In particular, a rigorous mathematical model, capable to quantify the CO₂ capture efficiency dynamics and the sorbent chemical composition during the process, is proposed for the first time. The model is validated by comparing modeling results with experimental data obtained under different operating conditions. The effect of both operating temperature and sorbent concentration are investigated. The good agreement between model results and experimental data confirms the effectiveness and the reliability of the developed tool that turns out to be able to quantify the dynamics of capture efficiency during the variation of the operating conditions. Therefore, it may be exploited to properly design, optimize and control the capture process and the absorbent regeneration section whose energy requirements also depend on the species concentration into the absorbent solution.

1. Introduction

The climate change, caused by the massive increase in anthropogenic greenhouse gas (GHG) emissions in recent decades, has become a serious environmental issue whose solution cannot be further delayed. Carbon dioxide (CO₂) is regarded as one of the most important GHGs, since its contribution from anthropogenic sources accounts for 74 % of the total GHGs [1], and the increase of its concentration in atmosphere has been correlated to the global warming observed since the middle of 20th century [2]. As a matter of fact, the atmospheric CO₂ concentrations climbed up dramatically in the past two centuries, rising from around 270 ppm in 1750 to current values higher than 410 ppm. To prevent a

further increase of the atmospheric CO₂ concentration, large stationary point sources of carbon dioxide such as power plants and refineries as well as iron, steel and cement industries should be suitably coupled with CCS (carbon capture and storage) [3] or CCU (carbon capture and utilization) [4,5] processes. This way, industrial CO₂ emissions could be reduced and transformed from a liability to an asset in a circular economy scenario. Nowadays, there are several technologies available for post combustion CO₂ capture including physical adsorption, chemical absorption, membrane processes, cryogenic separation, etc. [6]. Each technique displays its own advantages and drawbacks that depend on several factors such as temperature, pressure, volume of emissions to be treated, as well as CO₂ concentration and presence of humidity or other species in the flue gas [7,8].

* Corresponding authors at: Department of Mechanical, Chemical and Materials Engineering, University of Cagliari, Piazza d'Armi, 09123 Cagliari, Italy (Alessandro Concas).

E-mail addresses: f.atzori22@studenti.unica.it (F. Atzori), alessandro.concas@unica.it (A. Concas).

<https://doi.org/10.1016/j.cej.2022.138999>

Received 30 April 2022; Received in revised form 5 August 2022; Accepted 31 August 2022

Available online 7 September 2022

1385-8947/© 2022 The Authors. Published by Elsevier B.V. This is an open access article under the CC BY-NC-ND license (<http://creativecommons.org/licenses/by-nc-nd/4.0/>).

Nomenclature	
C_i	Concentration of the i^{th} species in the liquid bulk mol dm ⁻³
C_i^*	Equilibrium concentration of the i^{th} species mol dm ⁻³
$C_{w/T}$	Water concentration mol dm ⁻³
D	Diffusion coefficient dm ² s ⁻¹
D_b	Bubble diameter dm
D_C	Column diameter dm
d_0	Pore diameter of the sparger dm
d_{32}	Sauter mean diameter dm
E	Enhancement factor –
g	Gravity acceleration: 98.067 dm s ⁻²
H_C	Column height dm
H_D	Height of aerated liquid dm
H_S	Height of static liquid dm
H_i^j	Henry constant for i^{th} species in the j^{th} solvent Pa dm ³ mol ⁻¹
k_g	Local mass transfer coefficient for the gas phase mol Pa ⁻¹ dm ⁻² s ⁻¹
k_l	Local mass transfer coefficient for the liquid phase dm s ⁻¹
K_{R_i}	Equilibrium constant of the reaction R_i See Table 3
K_L	Global mass transfer coefficient dm s ⁻¹
MSE	Mean square error –
N_i	Gas/liquid interface molar flow rate of the i^{th} species mol s ⁻¹
N^{in}	Inlet molar gas flow rate mol s ⁻¹
N^{out}	Outlet molar gas flow rate mol s ⁻¹
N_{sc}	Schmidt number –
P	Pressure Pa
pH	pH level: $-\log_{10}([H^+])$ –
R	Gas constant: 8314.462 dm ³ Pa mol ⁻¹ K ⁻¹
R^2	Coefficient of determination –
S	Gas/liquid interface area dm ²
t	Time s
t_i	Sampling time of the efficiency measurement s
T	Temperature K
U_G	Bubble superficial velocity dm s ⁻¹
V_g	Gas-phase volume dm ³
V_L	Liquid-phase volume dm ³
y_i	Molar fraction of i^{th} species in the gas-phase –
ε	Liquid hold-up –
μ_l	Liquid phase dynamic viscosity kg dm ⁻¹ s ⁻¹
η	Capture system efficiency –
ν	Stoichiometric coefficient –
ρ_g	Gas phase-density kg dm ⁻³
ρ_l	Liquid phase-density kg dm ⁻³
$\Delta\rho$	Density difference between liquid- and gas-phase kg dm ⁻³
σ_l	Interfacial density of the liquid-phase kg s ⁻²
$\%_{c(i)}$	Concentration percentage ratio of the i^{th} species –

Chemical absorption is one of the most developed and feasible capture methods to reduce carbon dioxide emissions. In this technique, the flue gas is contacted with a liquid, usually an alkaline sorbent, to promote CO₂ dissolution and its subsequent reaction with the alkaline component, while the rest of the gaseous mixture is not retained. After the CO₂ capture, the absorbent solution can be thermally regenerated and reused in subsequent absorption cycles.

Due to its cost-effectiveness and the capability to handle large amount of emission, chemical absorption through aqueous alkanolamines is considered one of the most efficient capture methods and the most suitable for the revamping of existing plants. In particular, the use of aqueous monoethanolamine (MEA) has been extensively investigated in recent decades for CO₂ capture from large stationary emission points [9], and today it represents the most used absorbent in acid gas treatment [10,11]. However, the MEA process suffers from some severe disadvantages that prevent the capture system optimization. Specifically, low CO₂ loading capacity, high corrosion rate of equipment, amine thermal and oxidative degradation by SO₂, NO₂, HCl and HF as well as high energy consumption during absorbent regeneration [12] are the main factors currently hindering the wide application of MEA for carbon capture.

The formulation and choice of the liquid sorbent are indeed an important area of research since its chemical-physical properties considerably influence the capture process efficiency. Ideally, the absorbent should exhibit high reactivity with CO₂, low heat requirement for regeneration, low volatility, low toxicity, high loading capacity, resistance to degradation and, given its use on industrial scale, low cost. Aqueous ammonia (NH₃) displays many of these characteristics, and its potential use as a sustainable sorbent for CO₂ capture processes has recently gained increasing interest [13,14]. Compared to amine-based sorbents, aqueous ammonia presents several advantages: it is not affected by thermal and oxidative degradation even in the presence of other gases or impurities, it is less corrosive, it has better global availability (and lower cost) and its regeneration energy is much lower than that one of MEA process [15,16]. Moreover, this process can also capture multiple flue gas components (NO₂, NO_x, and CO₂) and produce added

value chemicals, such as ammonium sulfate, ammonium nitrate and ammonium bicarbonate that are widely used as fertilizers [17]. On the other hand, aqueous ammonia has two major drawbacks, namely the high volatility of NH₃ and its slow reaction with CO₂ [18], which must be considered and suitably managed to permit its large-scale implementation.

Despite the apparent simplicity of the system, most mathematical models so far available in the literature do simulate the concerned system only under equilibrium conditions. In particular, the equilibrium relations have been included into the so-called electrolyte non-random two liquid (NRTL) model [19–21]. Nevertheless, these models are not capable to describe the capture dynamics and the process evolution over time. For this reason, in this work, a novel mathematical model that manages to dynamically describe the CO₂ capture process is proposed for the first time, to the best of our knowledge. By considering reaction equilibria, the model allows computing the species concentration in the absorbent solution and to quantify the capture system efficiency as the process evolves. Such information could be very useful to identify the proper solvent regeneration times or to evaluate the possibility to integrate the process with the production of added-value chemicals, as well as to assess the operating conditions that optimize the CO₂ capture.

2. Materials and methods

All reagents were reagent grade and were used without further purification. The used aqueous NH₃ solutions were prepared from a standard 15.2 mol dm⁻³ of NH₃ solution (Sigma–Aldrich). Pure CO₂ and N₂ (Rivoira) were mixed together to simulate a flue gas with the desired composition (CO₂ 15 %_{v/v}). Flow rates of the gases were measured by means of digital gas mass flow controllers (Aalborg) equipped with gas flowmeters (Cole Parmer). The inlet and outlet CO₂ percentages in the flue gas mixture were measured with a Varian CP-4900 gas chromatograph calibrated with 10 %_{v/v} and 40 %_{v/v} CO₂/N₂ reference mixtures and 100 % CO₂ reference gas (Rivoira).

2.1. CO₂ capture experiments

The CO₂ capture was performed under isothermal and isobaric conditions in a home-built glass cylinder with a diameter of 56 mm and a height of 300 mm fitted with a sintered gas diffuser (16–40 μm) in the bottom. The absorber was charged with 0.150 dm³ of the tested aqueous ammonia solution and was kept at the desired temperature by means of a thermostatic bath (Julabo model F33 MC, accuracy ± 0.1 °C). The gas mixture was water-saturated before being injected from the bottom of the absorber through a sintered glass diffuser, with a total flow rate of 12.2 dm³h⁻¹ (0.076 mol_{CO₂}h⁻¹ at 23 °C). The vent gas from the top of the absorber was dried by flowing in turn through a condenser cooled at -5 °C, a concentrated H₂SO₄ solution and two towers filled with P₂O₅, before being GC analyzed. The gas chromatograph continuously measured the percentage of CO₂ in the treated gas stream. By comparing the percentage of CO₂ in the gas mixture before and after the absorption, the capture efficiency is calculated. Measurements of pH and temperature of the solution during absorption were performed with a HI98128 pHep®5 pH & temperature tester (Hanna Instruments, accuracy ± 0.05), calibrated with standard buffer solutions at pH 7.01 and 10.01. A schematic representation of the apparatus used is shown in Fig. 1.

The gas holdup (ϵ) is a key hydrodynamic factor to estimate the bubbles diameter. It was measured photographically, through the method of volume expansion, by recording the height of both the static (H_S) and aerated liquid (H_D), respectively before and after gas injection as follows: $\epsilon = (H_D - H_S)/H_D$. In order to validate the proposed model and verify its robustness, we conducted three different series of experiments, varying operational parameters such as the NH₃ initial concentration of the sorbent (M, mol dm⁻³) and the system temperature as summarized in Table 1.

2.2. ¹³C NMR analysis

The identification and quantification of the species formed during the capture process was obtained with an accurate ¹³C NMR analysis of solution samples taken after 10, 20, 30, 40, 60, 90, 120, 180, 240 and 300 min of absorption [22], following a well-established procedure [23]. The ¹³C NMR spectra were obtained with a Bruker Avance III 400 spectrometer, operating at 100.613 MHz. Tetramethylsilane was used as external standard at 0.00 ppm, while CH₃CN was used as internal reference (CH₃, $\delta = 1.47$). A sealed glass capillary containing D₂O (Sigma-Aldrich) was introduced into the NMR tube with the solution sample to provide a good signal for deuterium lock. A pulse sequence

Table 1

Operating conditions of the three different series of experiments.

	[NH ₃] ⁰ _[M]	T _[°C]
Exp.1	1.0	5
Exp.2	1.0	20
Exp.3	0.5	20

with proton decoupling and NOE suppression was used to acquire the ¹³C{¹H} with the following acquisition parameters: pulse angle = 90.0°, acquisition time = 1.3632 s, delay time = 2–30 s, data points = 65 K, number of scans = 250–500. The data were processed by Bruker-Biospin Topspin software. Bicarbonate and carbonate ions provide a unique ¹³C NMR signal, due to proton scrambling. The relative amount of ammonium carbamate (NH₂CO₂⁻) and of the sum of bicarbonate and carbonate (HCO₃⁻ + CO₃²⁻) was evaluated by comparing the intensities of their ¹³C NMR signals. The relative amount of bicarbonate and carbonate ions was evaluated from the chemical shift (δ , ppm) of the fast-equilibrating HCO₃⁻/CO₃²⁻ signal, as already described in a previous work [24]. Reference solutions for calibrating the ¹³C NMR spectra were prepared by dissolving in D₂O pure Na₂CO₃, NaHCO₃ and accurately weighted mixtures of the two salts in different percentages. Chemical shifts of reference solutions are in ppm and the percentages of Na₂CO₃ are reported in parenthesis: $\delta = 168.10$ (100 % neat Na₂CO₃); $\delta = 166.08$ (74.8 %); $\delta = 164.42$ (50.0 %); $\delta = 162.48$ (25.0 %); $\delta = 160.59$ (0 %, neat NaHCO₃).

3. Mathematical model

3.1. Gas/Liquid mass transfer

The strategy adopted to simulate the experimental results relies on the classical homogeneous model for unstirred bubble column tank reactors operated continuously for the gas phase and in batch mode for the liquid one. Isothermal and isobaric conditions are assumed, consistently with the experimental procedure. Due to the concentration gradient (driving force), carbon dioxide molecules diffuse from the gas bubbles to the liquid phase. In order to model this phenomenon, the two films theory is adopted. Rigorously, the reactive absorption process should be conceived by considering the film and the bulk sections for both phases along with the corresponding material balance equations for each of them. Therefore, the dynamic variation of the species concentrations results in a system of partial differential equations that takes into ac-

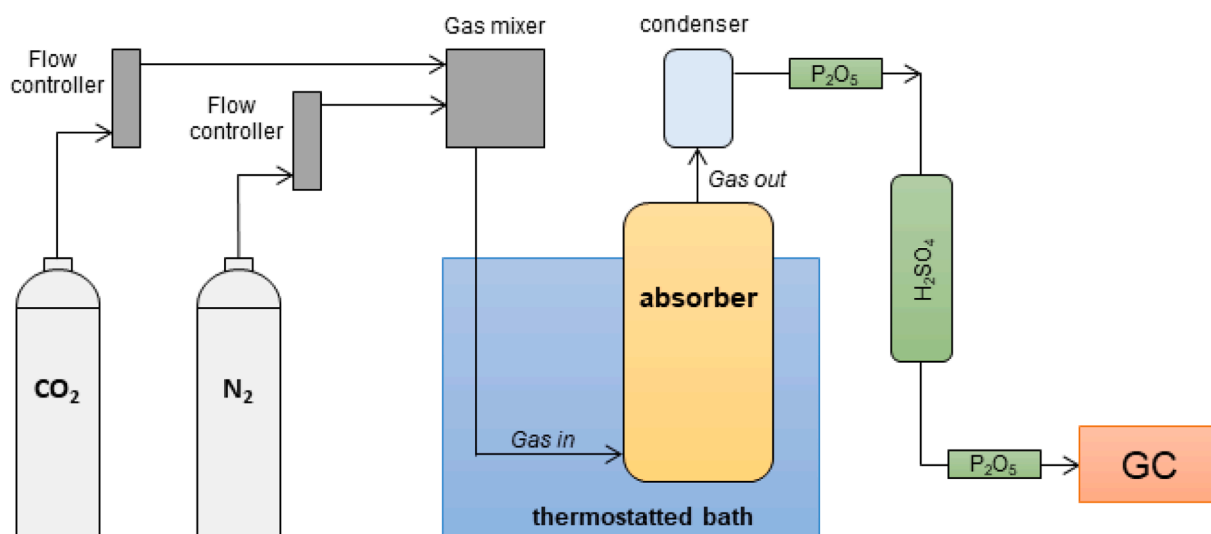


Fig. 1. Schematic diagram of the apparatus for CO₂ absorption experiments.

count the interface flow rate and the reactive phenomena taking place in the liquid phase. This model should be then coupled with the relevant boundary and initial conditions, related to bulk concentrations, the interface equilibrium and the molar transfer rate taking place at the gas/liquid interface. However, the unavailability of experimental data related to the time evolution of species concentration along the film, would make such a rigorous model uselessly complicated. For this reason, in this work, the CO_2 molar flow rate (N_{CO_2}), through the gas/liquid interface, is modelled by considering the global mass transfer coefficient, K_{LCO_2} and the enhancement factor, E , that describes the influence of a chemical reaction on the mass transfer rate:

$$N_{CO_2} = S E K_{LCO_2} (C_{CO_2}^* - C_{CO_2}). \quad (1)$$

where (C_{CO_2}) is the carbon dioxide concentration into the liquid bulk and ($C_{CO_2}^*$) represents its equilibrium concentration while the surface where mass transfer occurs is indicated by S .

To accurately describe the capture process, ammonia losses should also be considered and modelled via eq. (2):

$$N_{NH_3} = S K_{LNH_3} (C_{NH_3}^* - C_{NH_3}). \quad (2)$$

3.1.1. Henry constants

By relying on the Henry's law [25], the equilibrium concentration (C_i^*) of the i^{th} species can be evaluated through eq. (3) [26].

$$C_i^* = \frac{Py_i}{H_i^j}, \quad (3)$$

where P is the total pressure of the capture system, y_i is the molar fraction of the i^{th} species within the gas phase and H_i^j is the Henry constant for the i^{th} species in the j^{th} solvent.

The Henry constant of a specific gas is strictly dependent on solvent properties and system temperature. Eqs. (4) and (5) show the correlations adopted to evaluate the Henry constant of CO_2 ($H_{CO_2}^{H_2O}$) and NH_3 ($H_{NH_3}^{H_2O}$) in water, respectively as a function of temperature [27]:

$$H_{CO_2}^{H_2O} = \frac{1}{3.4} 10^4 \exp \left[-2350 \left(\frac{1}{T} - \frac{1}{298.15} \right) \right] \quad (4)$$

$$H_{NH_3}^{H_2O} = \frac{1}{0.59} \exp \left[-4200 \left(\frac{1}{T} - \frac{1}{298.15} \right) \right]. \quad (5)$$

The "N₂O analogy", proposed by [28] and expressed by eq. (6), is used to estimate the CO_2 solubility in water/ammonia solution, $H_{CO_2}^{w/a}$ [29]:

$$H_{CO_2}^{w/a} = H_{N_2O}^{w/a} \frac{H_{CO_2}^{H_2O}}{H_{N_2O}^{H_2O}}, \quad (6)$$

Where the N₂O Henry constant in water solution ($H_{N_2O}^{H_2O}$) can be expressed by eq. (7) [12]:

$$H_{N_2O}^{H_2O} = 8.55 \cdot 10^6 \exp \left[\frac{-2284}{T} \right], \quad (7)$$

and eq. (8) can be used to correlate $H_{N_2O}^{w/a}$ with ammonia concentration [30]:

$$H_{N_2O}^{w/a} = (0.155 + 8.17 \cdot 10^{-3} [NH_3]) \cdot 10^6 \exp \left[\frac{-1.14 \cdot 10^3}{T} \right]. \quad (8)$$

3.1.2. Enhancement factor

The enhancement factor (E) is defined as the ratio between the absorption rate of a gas component into a liquid phase in the presence of one or more reactions involving the absorbed gas species and the absorption rate when reactions are not taking place. However, it is well

known [31] that no general analytical expressions to calculate this value are available in the literature since it strictly depends on the reaction kinetics, the physiochemical properties of the species and the reaction regime. In this work, the approach proposed in the literature [31] is taken into account where the Hatta number, Ha (eq. (9)), and the enhancement factor infinite, E_{inf} (eq. (10)), are obtained to firstly determine the reactive regime occurring:

$$Ha = \frac{\sqrt{k_{app} D_{CO_2}}}{K_{LCO_2}} \quad (9)$$

$$E_{inf} = 1 + \left(\frac{D_{NH_3} [NH_3]}{\nu_{NH_3} D_{CO_2} \frac{Py_{CO_2}}{H_{CO_2}^{w/a}}} \right), \quad (10)$$

where k_{app} is the apparent kinetic constant of the reactive phenomena that determine the CO_2 consumption into the liquid phase [12,32,33], D_i is the diffusion coefficient of the i^{th} species and ν_{NH_3} is the ammonia stoichiometric coefficient in the reaction involving CO_2 consumption.

In this work, based on the experimental conditions, two different regimes are possible, i.e. the *pseudo first order* one that occurs when ammonia is in excess compared to CO_2 and the *fast intermediate regime* that takes place when CO_2 accumulates in the liquid phase [31].

If the *pseudo first order* condition is satisfied ($3 < Ha \ll E_{inf}$) [12,32,33], the enhancement factor can be computed through eq. (11):

$$E = \frac{Ha}{\tanh(Ha)} \quad (11)$$

As the process evolves, the absorption process falls into the *fast intermediate regime*, during which the enhancement factor can be approximate through the eq. (12) [34,35], proposed by [36] for the first time:

$$E = \frac{-Ha^2}{2(E_{inf} - 1)} + \sqrt{\frac{Ha^4}{4(E_{inf} - 1)^2} + \frac{E_{inf} Ha^2}{(E_{inf} - 1)} + 1}. \quad (12)$$

3.1.3. Mass transfer coefficient

The global mass transfer coefficient, K_L , as expressed by eq. (13), depends on both local transfer coefficients, i.e. k_l and k_g , that contribute to the global mass transfer resistance [37]:

$$\frac{1}{E K_L} = \frac{1}{E k_l} + \frac{1}{H_i^j k_g}. \quad (13)$$

Nevertheless, in the mass transfer model of bubble columns, the gas phase resistance is commonly assumed to be negligible ($Ek_l \ll k_g H_i^j$) [38–40], since the material transfer resistance is assumed to be concentrated in the homogeneous liquid-phase only ($K_L \rightarrow k_l$).

The local transfer coefficients expression is strictly dependent on the system configuration and geometry. By relying on experimental observations, some correlations for mass transfer coefficients have been developed for standard cases (e.g., fluid flow through a packed bed of particles, gas bubbles rising in a tank, falling films, flow over surfaces and within tubes). In this work, based on the configuration of the experimental setup, the correlation referring to rising gas bubbles reported in eq. (14) is used [26,41–42]:

$$k_l = \frac{2D}{D_b} + 0.31 N_{sc}^{-\frac{2}{3}} \left(\frac{\Delta \rho g \mu_l}{\rho_l^2} \right)^{\frac{1}{3}} \quad (14)$$

where D is the gas diffusion coefficient, N_{sc} is the Schmidt number, ρ_l and μ_l represent the liquid phase density and dynamic viscosity, respectively, the symbol $\Delta \rho$ accounts for the density difference between liquid and gas phase, g is the gravity acceleration and D_b is the bubble diameter.

Within the solution, the bubble size distribution is not uniform, due

to coalescence and break-up phenomena that are strongly influenced by the physical properties of the solution and the system fluid dynamics. As a consequence, the Sauter mean diameter (d_{32}) is considered to represent the average size of the bubbles [43]. By referring to the specific experimental condition such as type of sparger and column geometry, eq. (15), proposed by [44] to evaluate d_{32} , was selected:

$$d_{32} = d_0 \left(\frac{\rho_l}{\rho_g} \right)^{0.07271} \left(\frac{\sigma_l^3 \rho_l}{g \mu_l^4} \right)^{-0.04322} \left(\frac{H_C}{D_C} \right)^{0.16528} \left(\frac{U_G}{\sqrt{g D_C}} \right)^{0.27752} \left(\frac{d_0}{D_C} \right)^{-0.71397} \quad (15)$$

where d_0 is the pore diameter of the sparger, σ_l is the interfacial tension of the liquid, ρ_g is the gas density, H_C and D_C are the height and the diameter of the column whereas U_G is the superficial gas velocity, estimated by knowing the gas volumetric flow rate and the column section. The superficial gas velocity (U_G) could be then used to assess the theoretical hold-up (ϵ), through eq. (16), in order to compare the experimental value with the theoretical one:

$$\epsilon = \left(\frac{g D_C^2 \rho_l}{\sigma_l} \right)^{-1.167} \left(\frac{g \rho_l^2 D_C^3}{\mu_l^2} \right)^{0.3317} \left(\frac{U_G}{\sqrt{g D_C}} \right)^{0.3196} \left(\frac{\rho_l}{\rho_g} \right)^{1.048} \left(\frac{H_S}{D_C} \right)^{1.4948} \left(\frac{d_0}{D_C} \right)^{-0.862} \quad (16)$$

The relations used to quantify the physical properties of the system are reported in the [supplementary materials](#). Once the Sauter diameter is assessed, the interfacial surface, S , can be evaluated by multiplying the total bubble volume in the solution obtained from hold-up measurements and the bubble surface to volume ratio.

3.2. Reactive system

Once the CO_2 is dissolved, a series of chemical reactions takes place in the liquid phase. Carbon dioxide reacts with water and NH_3 producing carbonate, bicarbonate and carbamate ions [12] which could potentially give rise to heterogeneous reactions involving solid chemicals. In this work, the heterogeneous equilibria are neglected due to the high solu-

$$0 = [H^+] - \frac{K_w}{[H^+]} - \frac{K_1[CO_2]}{[H^+]} - 2 \frac{K_1 K_2 [CO_2]}{[H^+]^2} - \frac{K_4 K_1 [CO_2] [NH_3]}{[H^+]} + \frac{K_{am} [NH_3] [H_2O] [H^+]}{K_w} \quad (22)$$

bility of the species at stake [45–47]. The validity of this hypothesis depends on the specific operating conditions such as temperature and species concentration. Accordingly, the reactive system can be described by the reactions shown in [Table 2](#).

Based on the values of the Hatta number (eq. (9)), the reaction rate of the carbon dioxide consumption and the interface mass transfer rate are

Table 2

Main chemical reactions taking place in the liquid phase after CO_2 dissolution.

Reaction	ID
$CO_2 + H_2O \rightleftharpoons K_1 HCO_3^- + H^+$	R 1
$HCO_3^- \rightleftharpoons K_2 CO_3^{2-} + H^+$	R 2
$2NH_3 + CO_2 \rightleftharpoons K_3 NH_2CO_2^- + NH_4^+$	R 3
$NH_3 + HCO_3^- \rightleftharpoons K_4 NH_2CO_2^- + H_2O$	R 4
$NH_3 + H_2O \rightleftharpoons K_w NH_4^+ + OH^-$	R 5
$H_2O \rightleftharpoons K_w OH^- + H^+$	R 6

compared. Since the latter one results to be the rate limiting step, reactions (R 1–R 6) are considered to be instantaneous so that the corresponding equilibrium conditions are immediately reached. The equilibrium constant of R 1–R 6 and the corresponding relationship as a function of temperature are reported in [Table 3](#).

3.3. Model framework

The model used to describe the liquid phase is based on two specification equations. The total carbon, C_T (eq. (17)), and total nitrogen, N_T (eq. (18)), equations, that consider the chemicals in the reactions (R 1–R 6) involving carbon or nitrogen are reported as follows:

$$[C_T] = [CO_2] + [HCO_3^-] + [CO_3^{2-}] + [NH_2CO_2^-] \quad (17)$$

$$[N_T] = [NH_3] + [NH_4^+] + [NH_2CO_2^-] \quad (18)$$

Moreover, the latter ones may be combined with the following electroneutrality condition that accounts for the solution neutrality and

relates the ions concentrations into the solution:

$$0 = [H^+] - [OH^-] - [HCO_3^-] - 2[CO_3^{2-}] - [NH_2CO_2^-] + [NH_4^+] \quad (19)$$

Under the assumption that the reactions above are under equilibrium conditions, the total carbon concentration (eq. (17)), the total nitrogen concentration (eq. (18)) and the electroneutrality condition (eq. (19)) can be expressed in terms of $[CO_2]$, $[NH_3]$ and $[H^+]$, respectively as shown in the following equations:

$$[C_T] = [CO_2] + \frac{K_1[CO_2]}{[H^+]} + \frac{K_1 K_2 [CO_2]}{[H^+]^2} + \frac{K_3 K_w [CO_2] [NH_3]}{[H^+] [H_2O] K_{am}} \quad (20)$$

$$[N_T] = [NH_3] + \frac{K_{am} [NH_3] [H_2O] [H^+]}{K_w} + \frac{K_4 K_1 [CO_2] [NH_3]}{[H^+]} \quad (21)$$

During the capture process, the total carbon concentration is expected to vary along with the total nitrogen concentration. Due to CO_2 diffusion from the gas bubbles, $[C_T]$ increases until the solution is saturated, while the NH_3 evaporation phenomenon determines the $[N_T]$ decrease. By considering the liquid phase of the experimental bubble column perfectly mixed, the $[C_T]$ and $[N_T]$ time variation can be obtained from the following mass balances:

$$\frac{d[C_T]}{dt} = \frac{N_{CO_2}}{V_L} = \frac{S E K_{LCO_2}}{V_L} \left(\frac{P y_{CO_2}}{H_{CO_2}^{w/a}} - [CO_2] \right) \quad (23.1)$$

$$\frac{d[N_T]}{dt} = \frac{N_{NH_3}}{V_L} = \frac{S K_{LNH_3}}{V_L} \left(\frac{P y_{NH_3}}{H_{NH_3}^{w/a}} - [NH_3] \right), \quad (23.2)$$

where V_L is the volume of the liquid-phase. By deriving eq. (20), eq. (21) and eq. (22) with respect to the time and considering eq. (23.1) and

Table 3
Equilibrium constant.

Symbol	M.U.	$K_{eq}(T_{[K]})$	Reference
K_1	$[\text{mol L}^{-1}]$	$10^{\left(-\frac{3404.71}{T} + 14.8435 - 0.032786 T\right)}$	[48]
K_2	$[\text{mol L}^{-1}]$	$10^{\left(-\frac{2909.1}{T} + 6.119 - 0.02272 T\right)}$	[48]
K_3	$[\text{L mol}^{-1}]$	$C_{w/T} \cdot 10^{\left(+3.981 \frac{10^7}{T^3} - \frac{223620}{T^2} - \frac{348.71}{T} + 14.66 - 0.049 T + 0.65 \log(T)\right)}$	*
K_4	$[\text{L mol}^{-1}]$	$e^{\left(\frac{2900}{T} - 8.6\right)}$	[49]
K_{am}	$[-]$	$e^{\left(-\frac{3335.7}{T} - 1.257 - 0.037057 T + 1.497 \log(T)\right)}$	[50]
K_w	$[\text{mol}^2 \text{L}^{-2}]$	$10^{\left(-3.981 \frac{10^7}{T^3} + \frac{223620}{T^2} - \frac{3245.2}{T} - 4.098\right)}$	[51]

* K_3 is evaluated as reported in the supplementary materials.

eq. (23.2), the following expressions are obtained:

$$\begin{aligned} \frac{S E K_{LCO_2}}{V_L} \left(\frac{P y_{CO_2}}{H_{CO_2}^{w/a}} - [CO_2] \right) &= \frac{d[CO_2]}{dt} \left(1 + \frac{K_1}{[H^+]} + \frac{K_1 K_2}{[H^+]^2} \right. \\ &+ \frac{K_3 K_w [NH_3]}{[H^+][H_2O]K_{am}} \left. \right) + \frac{d[H^+]}{dt} \frac{[CO_2]}{[H^+]^2} \left(K_1 \right. \\ &+ \frac{2K_1 K_2}{[H^+]} + \frac{K_3 K_w [NH_3]}{[H_2O]K_{am}} \left. \right) \\ &+ \frac{d[NH_3]}{dt} \frac{K_3 K_w [CO_2]}{[H^+][H_2O]K_{am}} \end{aligned} \quad (24)$$

$$\begin{aligned} \frac{S K_{LNH_3}}{V_L} \left(\frac{P y_{NH_3}}{H_{NH_3}^{w/a}} - [NH_3] \right) &= \frac{d[CO_2]}{dt} \frac{K_4 K_1 [NH_3]}{[H^+]} + \\ &+ \frac{d[H^+]}{dt} \left(\frac{K_4 K_1 [NH_3][CO_2]}{[H^+]^2} - \frac{K_{am}[NH_3][H_2O]}{K_w} \right) \\ &+ \frac{d[NH_3]}{dt} \left(1 + \frac{K_{am}[H^+][H_2O]}{K_w} + \frac{K_4 K_1 [CO_2]}{[H^+]} \right) \end{aligned} \quad (25)$$

$$\begin{aligned} 0 &= \frac{d[CO_2]}{dt} \left(-\frac{K_4 K_1 [NH_3]}{[H^+]} - \frac{K_1}{[H^+]} - \frac{2K_1 K_2}{[H^+]^2} \right) + \\ &+ \frac{d[H^+]}{dt} \left(1 + \frac{K_w}{[H^+]^2} + \frac{K_{am}[NH_3][H_2O]}{K_w} + \frac{K_1 [CO_2]}{[H^+]^2} \right) \\ &\bullet \left(\frac{K_4 K_1 [NH_3][CO_2]}{[H^+]^2} + \frac{4K_1 K_2 [CO_2]}{[H^+]^3} \right) \\ &+ \frac{d[NH_3]}{dt} \left(\frac{K_{am}[H^+][H_2O]}{K_w} - \frac{K_4 K_1 [CO_2]}{[H^+]} \right) \end{aligned} \quad (26)$$

The above relations eqs. (24)–(26) could be seen as an algebraic third order linear system, where the unknowns are $x'_1 = \left[\frac{d[H^+]}{dt}, \frac{d[CO_2]}{dt}, \frac{d[NH_3]}{dt} \right]$ and the coefficients depend on the instantaneous concentration of the same species (x_1) as well as on the constant terms depend on x_1 and $x_g = [y_{CO_2}, y_{NH_3}]$. By solving this system, the expression for f_1, f_2 and f_3 that relate x'_1 to the state variable $x = [x_1, x_g]$ can be evaluated (as reported in the [Supplementary Materials](#)). To complete the model, the gas phase mass balances for NH_3 and CO_2 need to be accounted for. The resulting system of ODEs to be solved is reported in what follows:

$$\begin{aligned} \frac{dy_{CO_2}}{dt} &= \frac{RT}{PV_g} \left(N^{in} y_{CO_2}^{in} - N_{CO_2} - N^{out} y_{CO_2} \right); \\ y_{CO_2}(0) &= y_{CO_2}^0 \end{aligned} \quad (27)$$

$$\begin{aligned} \frac{dy_{NH_3}}{dt} &= \frac{RT}{PV_g} \left(-N_{NH_3} - N^{out} y_{NH_3} \right); \\ y_{NH_3}(0) &= y_{NH_3}^0 \end{aligned} \quad (28)$$

$$\begin{aligned} \frac{d[CO_2]}{dt} &= f_1([CO_2], [NH_3], [H^+], y_{CO_2}, y_{NH_3}); \\ [CO_2](0) &= [CO_2]^0 \end{aligned} \quad (29)$$

$$\begin{aligned} \frac{d[NH_3]}{dt} &= f_2([CO_2], [NH_3], [H^+], y_{CO_2}, y_{NH_3}); \\ [NH_3](0) &= [NH_3]^0 \end{aligned} \quad (30)$$

$$\begin{aligned} \frac{d[H^+]}{dt} &= f_3([CO_2], [NH_3], [H^+], y_{CO_2}, y_{NH_3}); \\ [H^+](0) &= [H^+]^0 \end{aligned} \quad (31)$$

where T is the temperature, R the gas constant, N^{in} and N^{out} are the inlet and outlet molar flow rate of the gas phase, respectively and V_g is

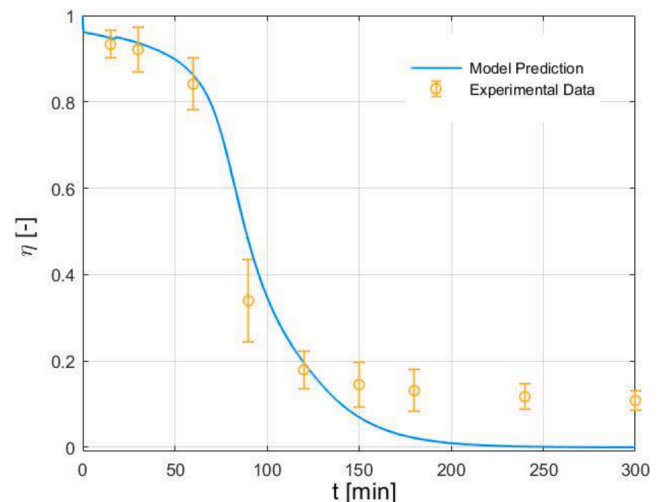


Fig. 2. Capture system efficiency, $[NH_3]^0 = 1.0 \text{ M}$, $T = 5 \text{ }^\circ\text{C}$ (Exp.1).

the gas-phase volume which accounts for the volume of bubbles and column headspace. Since the capture process is carried out under isothermal and isobaric conditions, the outlet molar flow rate of the gas phase could be computed as:

$$N^{out} = N^{in} - N_{CO_2} - N_{NH_3}. \quad (32)$$

The eqs. (27)-(31) allow to describe the CO_2 capture dynamics as well as the time evolution of $[CO_2]$, $[NH_3]$ and $[H^+]$. Once the concentrations of the latter ones are evaluated, those ones corresponding to the other species can be obtained through the equilibrium relations (R 1-R 6). The ODEs system above was solved through the subroutine ODE45 which takes advantage of the Runge-Kutta (4,5) method on Matlab.

4. Results and discussion

The model performance is evaluated by comparing the corresponding predictions with the experimental measurements related to the ion speciation, defined as the concentration ratio of ions within the solution, pH and capture system efficiency, defined by means of eq. (33):

$$\eta = \frac{N^{in} y_{CO_2}^{in} - N^{out} y_{CO_2}^{out}}{N^{in} y_{CO_2}^{in}}, \quad (33)$$

4.1. Experimental data and model predictions

Fig. 2 shows the capture efficiency experimental data of Exp.1 and the corresponding model predictions obtained without tuning any model parameter. During the first part of the experiment, the capture efficiency is close to unity because, due to the initial absence of dissolved CO_2 , the driving force reaches the highest possible values (eq. (1)). Consequently, the capture efficiency values (Fig. 2) show an initial phase (hereinafter referred to as “reaction phase”) where η slowly decreases since almost all the CO_2 transferred to the liquid phase is consumed by the dissolved ammonia. During this phase, the efficiency reduction is mainly caused by the enhancement factor decrease, due to ammonia consumption that influences the reaction rate [32,12]. As long as the ammonia level concentration allows to convert CO_2 , its accumulation into the liquid-phase is avoided and the CO_2 driving force in the liquid-phase remains unchanged. Once ammonia concentration starts decreasing, CO_2 starts to be accumulated in the liquid-phase and thus the corresponding driving force is reduced. Accordingly, the capture system efficiency significantly decreases until the CO_2 flow through the gas-liquid interface becomes quite small so that the corresponding η value drops below 20 %.

The statistical parameters $R^2(0.9708)$ [52] and $MSE(0.0441)$ [53], quantitatively confirm the model predictive capability that allows to capture fairly well the efficiency time dynamics, as shown with Fig. 2. During the last part, the model simulation underestimates the experimental data (Fig. 2). This offset could be due to an additional reactive phenomenon not accounted for by the model, which becomes relevant as the $[NH_3]$ is extremely low: one of the two ammonia molecules, needed to form $NH_2CO_2^-$ (R 3), is substituted by H_2O that serves as a base and promotes carbon dioxide consumption, thus limiting its accumulation in the final step of the process. However, the potential implication of such an offset should not be relevant in view of the transposition of the obtained results to the operative scale.

To the best of our knowledge, despite the simplicity of the reactive system, a model capable to describe the capture efficiency time evolution is not still available in the literature. In several works, the CO_2 - NH_3 - H_2O system is studied by means of the so-called electrolyte non-random two liquid (NRTL) model [19–21] that considers the equilibrium relations between the species and evaluates the species concentrations as a function of the CO_2 loading. However, the NRTL model is not capable to quantify the outlet CO_2 concentration (and thus the CO_2 capture efficiency), as a function of time. Moreover, even though some literature models take into account both the reaction process and the

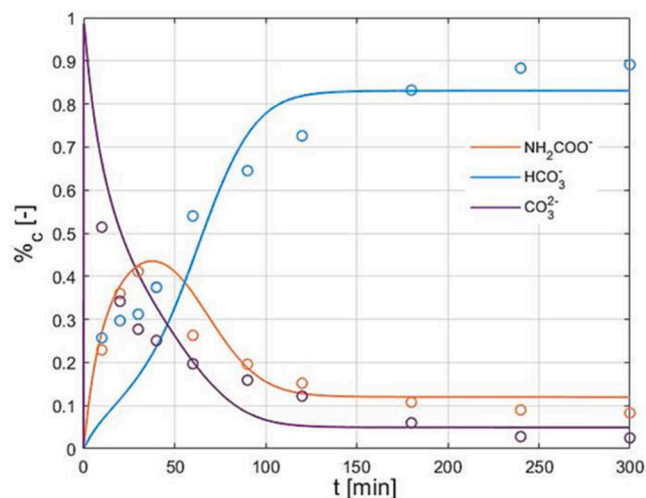


Fig. 3. Ion speciation. (o): exp. data, (-) model prediction (Exp.1).

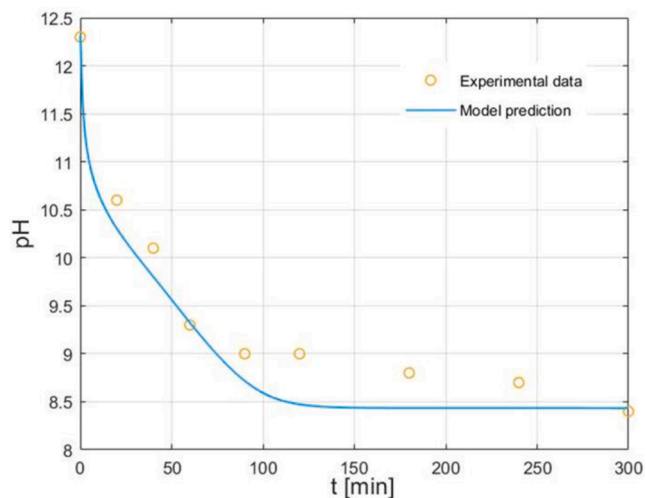


Fig. 4. pH variation during the capture process (Exp.1).

interface transfer phenomena, the quantitative description of the capture efficiency from the experimental results is typically missing [54].

To design an efficient plant for the chemical absorption of carbon dioxide, the capture system has to be integrated with a regeneration system which has the function to recycle the absorbent from the CO_2 -rich solution. The knowledge of the chemical composition of the CO_2 saturated solution could be the key to optimize the regeneration process since it permits to acquire data about the chemical and thermodynamic properties of the solution.

Fig. 3 shows how the chemical composition of the solution changes during the process. The experimental data related to the percentage concentration ratio of carbonate, (CO_3^{2-}), bicarbonate (HCO_3^-), and carbamate ($NH_2CO_2^-$) is reported, along with the corresponding model results.

During the first part of the experiment, the strong alkalinity of the solution moves reaction R 2 toward right, thus causing the exclusive production of carbonate ions (CO_3^{2-}) (Fig. 3). As the process evolves, the carbon content into the solution increases thus causing the increase of HCO_3^- concentration (R 1) and the decrease of pH (Fig. 4) that, in turn, gives rise to the shift of the R 2 equilibrium toward reagents. This phenomenon slows down the CO_3^{2-} formation and promotes the production of HCO_3^- and $NH_2CO_2^-$ (Fig. 3). The high NH_3 concentration in the early steps of the experiment determines the synthesis of $NH_2CO_2^-$

that is interrupted at the end of the initial reaction phase (Fig. 2), when the NH_3 content decreases. Moreover, the dissolved CO_2 causes a progressive $[H^+]$ increase (Fig. 4) that affects the chemical composition of the absorbent solution, thus favoring the HCO_3^- production, as the ammonia is consumed (Fig. 3).

The model turns out to be capable to predict the time evolution of CO_3^{2-}

($R^2 = 0.86, MSE = 0.009$), HCO_3^- ($R^2 = 0.79, MSE = 0.013$) and $NH_2CO_2^-$ ($R^2 = 0.90, MSE = 0.001$). The good accuracy of the predictions demonstrates the validity of the more significant hypotheses the model is based upon. The eqs. (27)-(31) are indeed solved by considering the species under equilibrium conditions (cf. reactions R 1-R 6), because the process is assumed to be under diffusive control.

During the base case experiment, also pH was measured. Within the first 90 minutes pH level decreases from 12.3 to 9, due to high CO_2 dissolution rate. When the solution approaches the corresponding level of CO_2 saturation, the pH variation slows down and its value levels off to about 8.5. The experimental $[H^+]$ evolution is well captured by the model ($R^2 = 0.94, MSE = 0.009$) via eq. (31) (Fig. 4).

4.2. Model validation

To further evaluate the predictive capability of the model, additional CO_2 absorption experiments were carried out under different operating conditions and the corresponding results were compared with the modeling ones. Since the thermal level significantly affects the reaction equilibrium and therefore the system dynamics, the capture process was carried out by changing the operating temperature to 20 °C (Exp. 2, Table 1). Especially when dealing with industrial scale absorption, the temperature is a parameter whose level is responsible for considerable energy consumption while operating at low temperatures is not always possible. Moreover, since the reactive absorption is an exothermic process, it is quite difficult to keep the temperature constant when large volumetric flow rate and reaction volumes are considered. Therefore, a model used to predict and describe the capture system dynamics should be efficient over a wide range of temperature. Fig. 5 deals with the comparison between experimental data and model predictions for the case of Exp. 2 where it is seen that the temperature change affects the capture system efficiency.

Fig. 5 shows how the reaction phase remains practically unchanged in terms of duration, with a slight increase of the corresponding values, due to the growth of the mass transfer rate with temperature. Nevertheless, the final decrease of η occurs more quickly than at 5 °C (Exp 1, Table 1) thus leading to values close to zero in 200 minutes. This is due

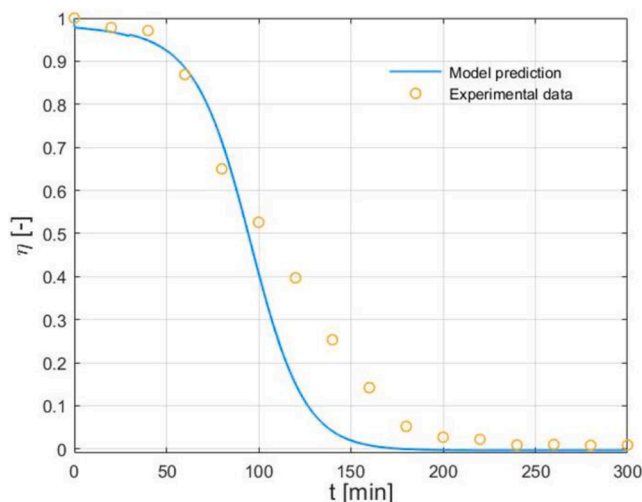


Fig. 5. Capture system efficiency, $[NH_3]^0 = 1.0$ M, $T = 20$ °C (Exp.2).

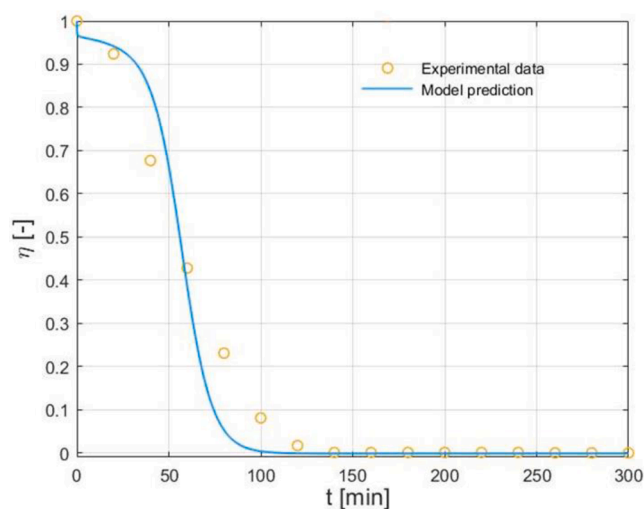


Fig. 6. Capture system efficiency, $[NH_3]^0 = 0.5$ M, $T = 20$ °C (Exp.3).

to the considerable decrease of K_3 (Table 3) that determines a faster accumulation of carbon dioxide into the liquid phase and the gas solubility reduction, due to the Henry constant decreasing, as shown in eq. (4), which causes the lowering of the saturation concentration. Accordingly, the reaction phase and the subsequent one are not negatively influenced by the temperature increase that, however, accelerates CO_2 accumulation and the efficiency reduction in the process final phase. For this reason, Fig. 5 presents a narrower offset with respect to Fig. 2.

The model was further validated by predicting the experimental results obtained when simultaneously varying initial ammonia concentration and process temperature (Exp. 3 in Table 1). Specifically, the initial NH_3 concentration was halved with respect to previous experiments (from 1.0 M to 0.5 M), while the temperature was set at 20 °C. The comparison between the model prediction and experimental results, in terms of capture efficiency, is reported in Fig. 6.

As expected, the halving of absorbent concentration has a remarkable influence on the reaction phase duration. In fact, the latter one is exclusively due to CO_2 consumption by NH_3 that prevents carbon dioxide accumulation within the solution. The lower is the initial concentration of ammonia, the faster is its consumption and the shorter is the reaction phase. Moreover, as also shown in Exp. 2 (Fig. 5), the temperature increase accelerates the solution saturation by attenuating the effects of secondary reaction phenomena and reducing the final mismatch between experimental and model results (Fig. 6).

The analysis of Fig. 5 and Fig. 6 shows the effectiveness and the reliability of the proposed mathematical model that is able to predict the absorption process dynamics despite the variation of the operating conditions. In Exp. 2 ($R^2 = 0.981, MSE = 0.003$) and Exp.3 ($R^2 = 0.975, MSE = 0.003$), respectively the data are fitted by the model curves quite well, by accurately describing the time evolution of the process efficiency. In particular, the developed model turns out to be able to predict how the temperature increase affects the process and to quantify the decrease of the reaction phase duration depending on the initial level of ammonia into the absorbent solution.

A validated model that effectively describes the reactive absorption process allows to gain important information in view of plant design. Based on the operating conditions, the time (hereafter called operation time) when the single absorber efficiency drops below a prescribed threshold can be evaluated. By computing, through the model, the operation time of a generic absorbent column, different plant configuration can be simulated. For instance, the model could be used to evaluate whether more columns should be operated in series, parallel or alternate configuration. Moreover, the "a priori" knowledge of the time evolution of the chemical composition might permit to properly design

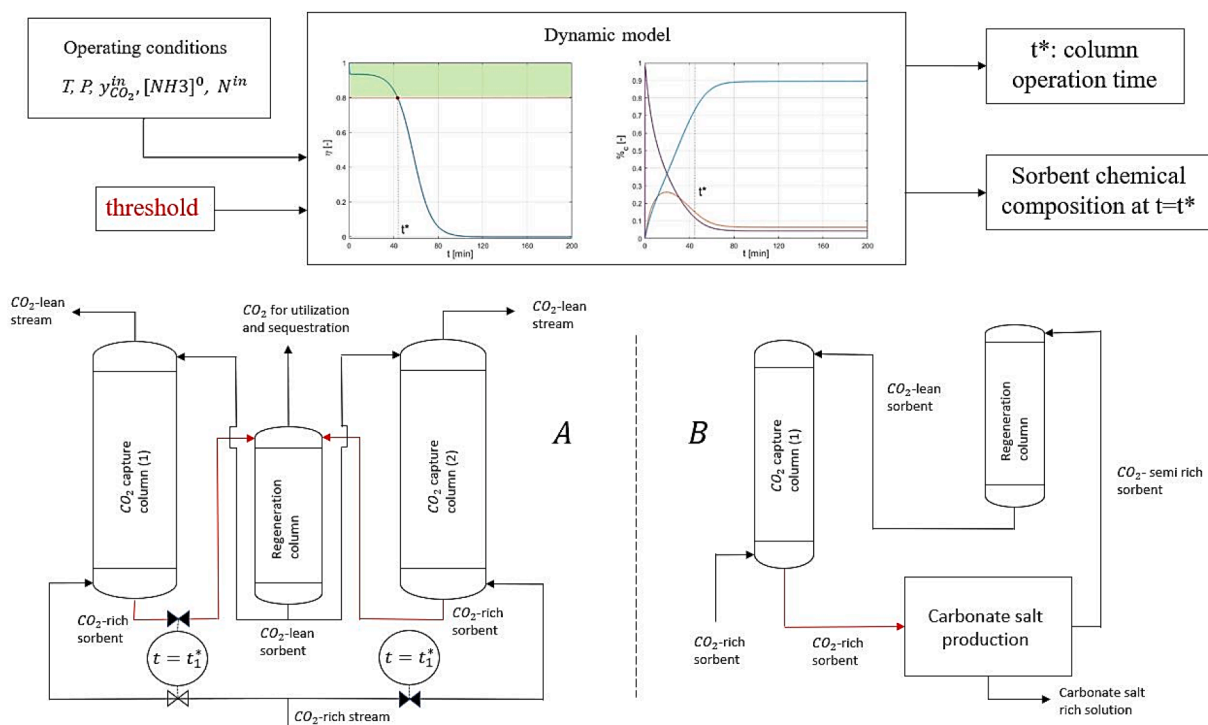


Fig. 7. Possible industrial applications of the proposed dynamic model.

the regeneration process as well as eventual intermediate steps of carbonate salts production.

Based on the consideration above, Fig. 7 shows two possible industrial application of the proposed mathematical model, which considers the two most significant model results: the column operation time (t^*) and the chemical composition analysis.

To this aim, let us consider two capture columns working alternatively (section A, Fig. 7) with the CO_2 -rich feed initially flowing only into column (1). Once t^* is selected depending upon operating conditions and threshold, the valve actuators can be programmed. The valve that controls the CO_2 -rich feed into the capture column (1) and the one controlling the CO_2 -rich feed into the capture column (2) can be closed and opened, respectively. Moreover, the valve that allows exhaust CO_2 -rich sorbent to flow in the regeneration column can be opened, without the use of real-time measurements.

In section B reports a potential application of the model related to its capability to predict the chemical composition of the solution is addressed. The CO_2 -rich sorbent solution can be seen as a raw material to synthesize carbonic salts in an intermediate production process whose yield also depends on the carbonic ion concentration. The proposed model could easily compute the chemical composition of the CO_2 -rich sorbent thus allowing one to utilize these data to design and optimize the carbonic salt production section.

As for the transposition of the results of this work at the industrial scale, it is worth mentioning that additional activities are required to simulate industrial conditions including suitable regeneration strategies depending upon the selected technologies where the knowledge of the corresponding hydrodynamics will affect the mass transfer coefficient values. However, the thermodynamics approach, adopted to describe the reactive absorption phenomenon, cannot be affected by the investigation scale since the speciation equations and the electroneutrality equation hold true even at larger scale. In addition, once the fluid dynamics is known, suitable expressions useful to evaluate the transfer coefficient can be identified while the mathematical structure of the proposed model equations remains unchanged.

5. Concluding remarks

In this work, a mathematical model able to quantitatively describe the dynamics of the CO_2 reactive absorption process with ammonia solutions is proposed for the first time. Based on reactions assumed to be under thermodynamical equilibrium and the gas/liquid CO_2 mass transfer occurrence, the model is capable to simulate the time variation of the system efficiency, the solution pH and the ion speciation in the liquid-phase, as the process evolves. The predictive capability of the model is successfully tested by comparison with experimental measurements related to capture efficiency, pH and ion speciation obtained under specific operating conditions ($T = 5\text{ }^\circ\text{C}$, $[NH_3]^0 = 1\text{ M}$).

A validation analysis is then carried out by comparing the model predictions with the experimental results obtained under different operating conditions. Initially, an experiment considering different system temperature ($T = 20\text{ }^\circ\text{C}$) is performed, while a simultaneous change in initial ammonia concentration and system temperature ($T = 20\text{ }^\circ\text{C}$, $[NH_3]^0 = 0.5\text{ M}$) is also considered. Despite the operating condition changes affects considerably the efficiency dynamics, the model is able to simulate the experimental trend, thus predicting the efficiency decrease due the temperature increase and the reduction of the reaction phase duration due to the lowering of ammonia concentration.

Such reliability makes the proposed mathematical model a useful tool in view of plant design. The use of the model could allow dynamic simulations to be carried out with different plant configurations, in order to identify the most advantageous ones. In addition, based on the chemical composition analysis, the optimization of the regeneration process and the integration of intermediate processes to produce added-value chemicals could be achieved.

Declaration of Competing Interest

The authors declare that they have no known competing financial interests or personal relationships that could have appeared to influence the work reported in this paper.

Data availability

Data will be made available on request.

Acknowledgement

CRS4 acknowledge the financial support of Regione Sardegna through the POR FESR Sardegna 2014–2020 structural fund.

Appendix A. Supplementary data

Supplementary data to this article can be found online at <https://doi.org/10.1016/j.cej.2022.138999>.

References

- [1] J. Olivier, J. Peters, Trends in global CO₂ and total greenhouse gas emissions, PBL Netherlands Environmental Assessment Agency: The Hague, The Netherlands. (2020).
- [2] B. Zhao, Y. Su, Y. Peng, Effect of reactor geometry on aqueous ammonia-based carbon dioxide capture in bubble column reactors, *Int. J. Greenhouse Gas Control* 17 (2013) 481–487, <https://doi.org/10.1016/j.ijggc.2013.06.009>.
- [3] T.A. Napp, A. Gambhir, T.P. Hills, N. Florin, P.S. Fennell, A review of the technologies, economics and policy instruments for decarbonising energy-intensive manufacturing industries, *Renew. Sustain. Energy Rev.* 30 (2014) 616–640, <https://doi.org/10.1016/j.rser.2013.10.036>.
- [4] M. Aresta, Carbon dioxide recovery and utilization, Springer Science & Business Media, 2003.
- [5] M. Aresta, A. Dibenedetto, A. Angelini, The changing paradigm in CO₂ utilization, *J. CO₂ Util.* 3–4 (2013) 65–73, <https://doi.org/10.1016/j.jcou.2013.08.001>.
- [6] F. Raganati, F. Miccio, P. Ammendola, Adsorption of carbon dioxide for post-combustion capture: A Review, *Energy Fuels* 35 (2021) 12845–12868, <https://doi.org/10.1021/acs.energyfuels.1c01618>.
- [7] R.M. Cuéllar-Franca, A. Azapagic, Carbon capture, storage and utilisation technologies: A critical analysis and comparison of their life cycle environmental impacts, *J. CO₂ Util.* 9 (2015) 82–102, <https://doi.org/10.1016/j.jcou.2014.12.001>.
- [8] I. Ghiat, T. Al-Ansari, A review of carbon capture and utilisation as a CO₂ abatement opportunity within the EWF nexus, *J. CO₂ Util.* 45 (2021), <https://doi.org/10.1016/j.jcou.2020.101432>.
- [9] X. Chen, G. Huang, C. An, Y. Yao, S. Zhao, Emerging N-nitrosamines and N-nitramines from amine-based post-combustion CO₂ capture – A review, *Chem. Eng. J.* 335 (2018) 921–935, <https://doi.org/10.1016/j.cej.2017.11.032>.
- [10] S. Singto, T. Supap, R. Idem, P. Tontiwachwuthikul, S. Tantayanon, M.J. Al-Marri, A. Benamor, Synthesis of new amines for enhanced carbon dioxide (CO₂) capture performance: The effect of chemical structure on equilibrium solubility, cyclic capacity, kinetics of absorption and regeneration, and heats of absorption and regeneration, *Sep. Purif. Technol.* 167 (2016) 97–107, <https://doi.org/10.1016/j.seppur.2016.05.002>.
- [11] X. Luo, S. Liu, H. Gao, H. Liao, P. Tontiwachwuthikul, Z. Liang, An improved fast screening method for single and blended amine-based solvents for post-combustion CO₂ capture, *Sep. Purif. Technol.* 169 (2016) 279–288, <https://doi.org/10.1016/j.seppur.2016.06.018>.
- [12] F. Qin, S. Wang, A. Hartono, H.F. Svendsen, C. Chen, Kinetics of CO₂ absorption in aqueous ammonia solution, *Int. J. Greenhouse Gas Control* 4 (2010) 729–738, <https://doi.org/10.1016/j.ijggc.2010.04.010>.
- [13] J.F. Pérez-Calvo, D. Sutter, M. Gazzani, M. Mazzotti, Advanced configurations for post-combustion CO₂ capture processes using an aqueous ammonia solution as absorbent, *Sep. Purif. Technol.* 274 (2021), <https://doi.org/10.1016/j.seppur.2021.118959>.
- [14] K. Villeneuve, D. Roizard, J.C. Remigy, M. Iacono, S. Rode, CO₂ capture by aqueous ammonia with hollow fiber membrane contactors: Gas phase reactions and performance stability, *Sep. Purif. Technol.* 199 (2018) 189–197, <https://doi.org/10.1016/j.seppur.2018.01.052>.
- [15] J.T. Yeh, K.P. Resnik, K. Rygle, H.W. Pennline, Semi-batch absorption and regeneration studies for CO₂ capture by aqueous ammonia, in: *Fuel Process. Technol.* (2005) 1533–1546, <https://doi.org/10.1016/j.fuproc.2005.01.015>.
- [16] A.C. Yeh, H. Bai, Comparison of ammonia and monoethanolamine solvents to reduce CO₂ greenhouse gas emissions, *Sci. Total Environ.* 228 (1999) 121–133.
- [17] F. Barzagli, F. Mani, M. Peruzzini, Carbon dioxide uptake as ammonia and amine carbamates and their efficient conversion into urea and 1,3-disubstituted ureas, *J. CO₂ Util.* 13 (2016) 81–89, <https://doi.org/10.1016/j.jcou.2015.12.006>.
- [18] H. Jilivero, F. Normann, K. Andersson, F. Johnsson, The rate of CO₂ absorption in ammonia-implications on absorber design, *Ind. Eng. Chem. Res.* 53 (2014) 6750–6758, <https://doi.org/10.1021/ie403346a>.
- [19] G. Qi, S. Wang, H. Yu, L. Wardhaugh, P. Feron, C. Chen, Development of a rate-based model for CO₂ absorption using aqueous NH₃ in a packed column, *Int. J. Greenhouse Gas Control* 17 (2013) 450–461, <https://doi.org/10.1016/j.ijggc.2013.05.027>.
- [20] H. Que, C.C. Chen, Thermodynamic modeling of the NH₃-CO₂-H₂O system with electrolyte NRTL model, *Ind. Eng. Chem. Res.* 50 (2011) 11406–11421, <https://doi.org/10.1021/ie201276m>.
- [21] P.M. Mathias, S. Reddy, J.P. O'Connell, Quantitative evaluation of the chilled-ammonia process for CO₂ capture using thermodynamic analysis and process simulation, *Int. J. Greenhouse Gas Control* 4 (2010) 174–179, <https://doi.org/10.1016/j.ijggc.2009.09.016>.
- [22] X.E. Hu, Q. Yu, F. Barzagli, C. Li, M. Fan, K.A.M. Gasem, X. Zhang, E. Shiko, M. Tian, X. Luo, Z. Zeng, Y. Liu, R. Zhang, NMR techniques and prediction models for the analysis of species formed in CO₂ capture processes with amine-based sorbents: A critical review, *ACS Sustainable Chem. Eng.* 8 (2020) 6173–6193, <https://doi.org/10.1021/acssuschemeng.9b07823>.
- [23] F. Barzagli, S. Lai, F. Mani, CO₂ capture by liquid solvents and their regeneration by thermal decomposition of the solid carbonated derivatives, *Chem. Eng. Technol.* 36 (2013) 1847–1852, <https://doi.org/10.1002/ceat.201300225>.
- [24] F. Barzagli, C. Giorgi, F. Mani, M. Peruzzini, CO₂ capture by aqueous Na₂CO₃ integrated with high-quality CaCO₃ formation and pure CO₂ release at room conditions, *J. CO₂ Util.* 22 (2017) 346–354, <https://doi.org/10.1016/j.jcou.2017.10.016>.
- [25] R.M. Rosenberg, W.L. Peticolas, Henry's law: a retrospective, *J. Chem. Educ.* 81 (2004) 1647.
- [26] R.H. Perry, D.W. Green, J.O. Maloney, *Perry's chemical engineers' handbook*, McGraw-Hill (1997).
- [27] R. Sander, Compilation of Henry's law constants (version 4.0) for water as solvent, *Atmos. Chem. Phys.* 15 (2015) 4399–4981, <https://doi.org/10.5194/acp-15-4399-2015>.
- [28] G.F. Versteeg, W.P. van Swaaij, Solubility and diffusivity of acid gases (carbon dioxide, nitrous oxide) in aqueous alkanolamine solutions, *J. Chem. Eng. Data* 33 (1988) 29–34.
- [29] M. Mehdipour, P. Keshavarz, A. Seraji, S. Masoumi, Performance analysis of ammonia solution for CO₂ capture using microporous membrane contactors, *Int. J. Greenhouse Gas Control* 31 (2014) 16–24, <https://doi.org/10.1016/j.ijggc.2014.09.017>.
- [30] J.B. Seo, S. bin Jeon, S.S. Lee, J.Y. Kim, K.J. Oh, The physical solubilities and diffusivities of N₂O and CO₂ in aqueous ammonia solutions on the additions of AMP, glycerol and ethylene glycol, *Korean J. Chem. Eng.* 28 (2011) 1698–1705, <https://doi.org/10.1007/s11814-011-0030-8>.
- [31] H. Kierzkowska-Pawlak, Determination of kinetics in gas-liquid reaction systems an overview, *Ecol. Chem. Eng. S.* 19 (2012) 175–196, <https://doi.org/10.2478/v10216-011-0014-y>.
- [32] P.W.J. Derks, G.F. Versteeg, Kinetics of absorption of carbon dioxide in aqueous ammonia solutions, in: *Energy Procedia*, 2009: pp. 1139–1146. 10.1016/j.egypro.2009.01.150.
- [33] J. Liu, S. Wang, G. Qi, B. Zhao, C. Chen, Kinetics and mass transfer of carbon dioxide absorption into aqueous ammonia, in: *Energy Procedia*, Elsevier Ltd, 2011: pp. 525–532. 10.1016/j.egypro.2011.01.084.
- [34] L.M. Galán Sánchez, G.W. Meindersma, A.B. de Haan, Kinetics of absorption of CO₂ in amino-functionalized ionic liquids, *Chem. Eng. J.* 166 (2011) 1104–1115, <https://doi.org/10.1016/j.cej.2010.12.016>.
- [35] F. Cao, H. Gao, H. Ling, Y. Huang, Z. Liang, Theoretical modeling of the mass transfer performance of CO₂ absorption into DEAB solution in hollow fiber membrane contactor, *J. Membr. Sci.* 593 (2020), <https://doi.org/10.1016/j.memsci.2019.117439>.
- [36] W.J. Doursey, *Absorption with chemical reaction: development of a new relation for the danckwerts model*, Pergamon Press (1974).
- [37] Y. Xu, B. Jin, Y. Zhao, E.J. Hu, X. Chen, X. Li, Numerical simulation of aqueous ammonia-based CO₂ absorption in a sprayer tower: an integrated model combining gas-liquid hydrodynamics and chemistry, *Appl. Energy* 211 (2018) 318–333, <https://doi.org/10.1016/j.apenergy.2017.11.054>.
- [38] R.B. Bird, W.E. Stewart, E.N. Lightfoot, *Transport Phenomena*, second, New York, 2002.
- [39] K. Nigar, B. Fahir, O.U. Kutlu, *Bubble column reactors*, *Process Biochemistry.* 40 (2005) 2263–2283.
- [40] G. Besagni, F. Inzoli, T. Ziegenhein, Two-phase bubble columns: a comprehensive review, *ChemEngineering.* (2018), <https://doi.org/10.3390/2020013>.
- [41] E.L. Cussler, *Diffusion Mass Transfer in Fluid systems*, Third edition (2007) www.cambridge.org/cussler.
- [42] J.M. Lee, *Biochemical Engineering*, 2009. <http://jmlee.net>.
- [43] R. Pohorecki, W. Moniuk, P. Bielski, P. Sobieszuk, G. Dąbrowiecki, Bubble diameter correlation via numerical experiment, *Chem. Eng. J.* 113 (2005) 35–39, <https://doi.org/10.1016/j.cej.2005.08.007>.
- [44] M. Abro, L. Yu, G. Yu, X. Chen, A.B. Qazi, Experimental investigation of hydrodynamic parameters and bubble characteristics in CO₂ absorption column using pure ionic liquid and binary mixtures: Effect of porous sparger and operating conditions, *Chem. Eng. Sci.* 229 (2021), <https://doi.org/10.1016/j.ces.2020.116041>.
- [45] F. Milella, M. Mazzotti, Estimation of the growth and the dissolution kinetics of ammonium bicarbonate in aqueous ammonia solutions from batch crystallization experiments, *Cryst. Growth Des.* 19 (2019) 5907–5922, <https://doi.org/10.1021/acs.cgd.9b00941>.
- [46] F. Barzagli, F. Mani, M. Peruzzini, From greenhouse gas to feedstock: Formation of ammonium carbamate from CO₂ and NH₃ in organic solvents and its catalytic conversion into urea under mild conditions, *Green Chem.* 13 (2011) 1267–1274, <https://doi.org/10.1039/c0gc00674b>.

- [47] F. Mani, M. Peruzzini, P. Stoppioni, CO₂ absorption by aqueous NH₃ solutions: Speciation of ammonium carbamate, bicarbonate and carbonate by a ¹³C NMR study, *Green Chem.* 8 (2006) 995–1000, <https://doi.org/10.1039/b602051h>.
- [48] D.D. Perrin, Dissociation constants of inorganic acids and bases in aqueous solution, *Pure Appl. Chem.* 20 (1969) 133–236.
- [49] T. Edwards, G. Maurer, J. Newman, J. Prausnitz, Vapor-liquid equilibria in multicomponent aqueous solutions of volatile weak electrolytes, *AIChE J.* 24 (1978) 966–976.
- [50] K. Li, H. Yu, G. Qi, P. Feron, M. Tade, J. Yu, S. Wang, Rate-based modelling of combined SO₂ removal and NH₃ recycling integrated with an aqueous NH₃-based CO₂ capture process, *Appl. Energy* 148 (2015) 66–77, <https://doi.org/10.1016/j.apenergy.2015.03.060>.
- [51] W.L. Marshall, E.U. Franck, Ion product of water substance, 0–1000 °C, 1–10,000 bars New International Formulation and its background, *J. Phys. Chem. Ref. Data* 10 (1983) 295–304, <https://doi.org/10.1063/1.555643>.
- [52] G. Cogoni, D. Widenski, M. Grosso, R. Baratti, J.A. Romagnoli, A qualitative comparison between population balances and stochastic models for non-isothermal antisolvent crystallization processes, *Comput. Chem. Eng.* 63 (2014) 82–90, <https://doi.org/10.1016/j.compchemeng.2014.01.001>.
- [53] C. Carotenuto, M. Grosso, P.L. Maffettone, Fourier transform rheology of dilute immiscible polymer blends: a novel procedure to probe blend morphology, *Macromolecules* 41 (2008) 4492–4500, <https://doi.org/10.1021/ma800540n>.
- [54] F. Chu, L. Yang, X. Du, Y. Yang, Mass transfer and energy consumption for CO₂ absorption by ammonia solution in bubble column, *Appl. Energy* 190 (2017) 1068–1080, <https://doi.org/10.1016/j.apenergy.2017.01.027>.